PROCEEDINGS, Eighteenth Workshop on Geothermal Reservoir Engineering
Stanford University, Stanford, California, January 26-28, 1993
SGP-TR-145

NUMERICAL MODELING OF INJECTION EXPERIMENTS AT THE GEYSERS

Karsten Pruess‡ and Steve Enedy†

‡Earth Sciences Division, Lawrence Berkeley Laboratory
University of California, Berkeley, CA 94720

†Northern California Power Agency, P.O. Box 663,
Middletown, CA 95461

ABSTRACT

Data from injection experiments in the southeast Geysers are presented that show strong interference (both negative and positive) with a neighboring production well. Conceptual and numerical models are developed that explain the negative interference (decline of production rate) in terms of heat transfer limitations and water-vapor relative permeability effects. Recovery and over-recovery following injection shut-in are attributed to boiling of injected fluid, with heat of vaporization provided by the reservoir rocks.

INTRODUCTION

Since the mid-eighties, reservoir pressures and well production rates at The Geysers have entered a period of accelerated decline (Goyal and Box, 1990; Enedy, 1992). Steam shortfalls have curtailed power generation, and have emphasized the need to view injection not just as a means for condensate disposal, but as a reservoir management tool for replenishing dwindling fluid reserves and enhancing energy recovery.

Injection design and interpretation of monitoring data require an understanding of the important reservoir processes. Using detailed data from a series of injection experiments in the southeast Geysers, we attempt to identify fluid and heat flow processes and geometric controls that determine reservoir response to injection.

INJECTION EXPERIMENTS

Recent injection experiments performed by NCPA in the Southeast Geysers have shown dramatic patterns of interference with production. During 1990 water was injected into well Q-2 for periods of from one day to several weeks at rates of 200-600 gpm (approximately 12-36 kg/s). Nearby production well Q-6 responded to injection with rapid strong rate declines. When injection was stopped production not only recovered but over-recovered. As shown in Figure 1, the interference pattern could be repeated over many injection cycles, and (over-) recovery of production was stronger for longer periods of injection shut-in.

Wells Q-2 and Q-6 are located in the north-central portion of the NCPA steam field near the lease line with Calpine's Unit 16 steam field. The wells are completed within the Franciscan graywacke, a metamorphosed sandstone. Greenstone segments within the graywacke serve as a secondary host rock. The main reservoir is overlain by a heterogeneous mixture of rock types which is set behind casing. The entire study area is underlain by a silicic intrusive known as the felsite; although neither Q-2 or Q-6 are drilled deep enough to reach the felsite. The wells are surrounded on all sides by steam production wells which are in hydraulic communication with both wells based on deuterium distribution (Beall et al., 1989) and static pressure analysis.

Prior to 1987, Q-2 was the primary injector for NCPA's Plant #2 with injection rates ranging from 800 to 2,000 gpm. Following the drilling and subsequent completion of several steam wells including Q-6 in 1987, the amount of injection into Q-2 was considerably reduced due to communication with offset steam wells. During 1990, Q-2 served as one of five injection wells utilized to inject condensate in the NCPA steam field and one of 34 injection wells used at The Geysers. Injection rates were normally limited to 200 to 600 gpm in order to minimize the amount of communication with the offset wells. The location of the wells within the field along with the relative volume of water injected into each Geyser injection well is shown in Figure 2.

Wells Q-2 and Q-6 are both directionally drilled. Q-6 is a type of non-conventional well completion known as a "forked hole" which is a well with two legs open to steam production. Both wells have multiple steam entries at depths between 1,300-2,000 m (4,265-6,562 ft) with typical spacing between steam entries of 100 m (328 ft). The distance between steam feeds in Q-2 and those in either leg of Q-6 range from 200-800 m (656-2,625 ft). A plan view and cross-section is shown in Figure 3.

Injection into Q-2 also caused interference with Calpine well 9589, which is located approximately 300 m (984 ft) due north of Q-2 (Tom Box, private communication). Initial effects were beneficial, increasing production rates, but later water breakthrough was observed.

The striking patterns of injection interference between wells Q-2 and Q-6 call for an explanation. In an attempt to identify reservoir conditions and processes that could cause such behavior, we first develop hypothetical models that may be capable of explaining the observations. Subsequently the viability of proposed models is evaluated by means of numerical simulation, and conclusions are drawn for design and monitoring of injection systems.

CONCEPTUAL MODEL

The strength and rapidity of interference between Q-2 and Q-6 suggests that both wells intersect some of the same fractures or fracture zones. These fractures would accept much of the fluid injected into Q-2, and provide important paths for flow of reservoir vapor to well Q-6 steam entries. During injection a plume of heating and partially boiling liquid will spread around the injection well. Depending on rates of fluid injection, and heat transfer from the reservoir rocks to the injection plume, two-phase zones with declining temperatures may develop. Because of the one-to-one correspondence between temperatures and pressures in two-phase conditions, fluid pressures in parts of the injection plume and the surrounding reservoir may decline, causing flow rate declines in neighboring wells. In addition, injected liquid in the fractures may partially block the vapor flow paths from the reservoir "at large" to well Q-6 feeds. This interference of injection-derived liquid with vapor flow can be thought of as a relative permeability effect.

After injection is stopped the injected liquid will, in part, boil away, migrate to greater depth, or be sucked by capillary force away from the fractures into the low-permeability rock matrix. Removal of the liquid will clear the fracture flow paths for vapor, causing production to recover. The observed over-recovery indicates that the injected liquid becomes available as a significant additional source of steam, boiling close to Q-6 ("close" in the sense of good hydraulic communication), with excellent access to reservoir heat. Heat transfer to the fluid could occur either by conduction to the fractures, with fluid boiling in the fractures, or injected liquid could be imbibed into the rock matrix, boiling there from local heat exchange.

Based on the foregoing discussion, the most important component in the model will be the fracture(s) by which Q-2 and Q-6 are connected. The fractures will take a portion of the fluid injected into Q-2, and will supply part of the production to Q-6. They will be coupled to matrix rock of small but finite permeability, that will transfer heat to the fluids in the fractures by conduction, while absorbing liquid from the fractures by capillary force. In addition to the specific fractures that connect Q-2 and Q-6, there is a general "background" reservoir that supplies long-term production to the local fracture system, and may also absorb some of the injected fluid.

The nature of the fracture system at The Geysers has been discussed in recent papers by Beall and Box (1989) and Thompson and Gunderson (1992). Both sub-horizontal and sub-vertical fractures are present. In the southeast Geysers high-angle (nearly vertical) fractures are thought to dominate. Monitoring of natural tracers (deuterium) in the southeast Geysers showed that injected fluids migrate primarily in north-south direction (Beall et al., 1989). The available information from the field does not provide the detailed geometry of the local fracture system on the scale of the distance between Q-2 and Q-6 feeds, of order 300m (984 ft). Our approach is to start with the simplest assumptions and flow geometries that would seem capable of explaining the strong and rapid negative production interference during injection, and the (over-)recovery following injection shut-in. Our modeling assumptions will then be revised and refined as needed to reduce discrepancies between predicted and observed behavior. The most "stripped down" model would seem to need two essential ingredients: (i) a single fracture intersecting both Q-2 and Q-6, and (ii) a large "background reservoir" connected to this fracture. Even in this most simplified model the flow geometry would be three-dimensional, and fluid and heat flows would need to be considered over a very large range of thermo-hydrologic parameters and spatial scales. Indeed, permeabilities range from microdarcies in the rock matrix to perhaps tens or hundreds of darcies in the fractures. Relevant spatial scales for the important flow processes are of the order of centimeters for flow in the fractures and imbibition into the rock matrix, several decimeters for penetration of heat conduction into wall rock over several days, and hundreds of meters for reservoir perturbation from long-term production. When coupled with the extremely non-linear process complexities of two-phase vaporizing flows, this leads to impractical computational demands, and further simplifications must be made.

Flow geometry can be simplified by modeling the fracture and the background reservoir as two separate two-dimensional systems with appropriate coupling, although in reality the local fractures are of course embedded in the reservoir. The background reservoir is modeled as a large radially-symmetric layered (R-Z) system. The fracture is modeled as a rectangular vertical (X-Z) section. Although the fracture itself requires only 2-D gridding, consideration of fluid and heat flow between the fracture and the surrounding reservoir rock will still make the system three-dimensional.

NUMERICAL SIMULATION APPROACH

A schematic of our fracture-reservoir flow model is shown in Fig. 4; the model parameters are summarized in Table 1. These parameters were not specifically selected for the local conditions in the study area; rather, they are intended to be generically applicable to The Geysers reservoir. Generally speaking, hydrologic parameters needed for two-phase flow modeling are not well known for Geysers rocks. As in previous studies of vapor-dominated reservoirs (Pruess and O'Sullivan, 1992), we have borrowed data for welded tuffs from nuclear-waste related studies (Peters et al., 1984). Welded tuffs have permeabilities in the microdarcy or fraction-of-a -microdarcy range, and are believed to have similar capillary and relative permeability behavior as unfractured graywacke or felsite from The Geysers.

We have modeled vertical fractures of different total area, from 300 x 300 to 600 x 600 m^2 (984 x 984 to 1969 x 1969 sq. ft). The fracture is modeled as a high-permeability porous medium with a small effective void space thickness of 1 cm (.39 in.), and a permeability-thickness product of 40 dm (131,200 millidarcy-ft). Relative permeability and capillary pressure behavior of fractures is not well known. Recent theoretical and experimental studies by Pruess and Tsang (1990) and Persoff et al. (1991) have suggested that two-phase flow behavior of fractures may be similar to that of three-dimensional porous media of high permeability. We have assumed that fracture capillary pressures are negligibly small, and that relative permeabilities may be represented by standard Corey-curves.

The distance between injection and production well is 240 m (787 ft). The background reservoir is modeled as a layered porous cylinder of 500 m (1640 ft) height and 1,000 m (3281 ft) radius. It is conceptualized as a dual-permeability fractured porous medium with average porosity of 4% and a total permeability-thickness product of 21.6 dm (70,866 millidarcy ft). Dual permeability behavior is modeled with an "effective porous medium" description. Chiefly, this consists of an effective relative permeability with a very high (80%) irreducible liquid saturation (Pruess and Narasimhan, 1982; Pruess, 1983a). The "background reservoir" serves as a means to provide stabilized long-term flow to the local fractures; simulated injection interference is not sensitive to detailed specifications of the background reservoir.

As a starting point for simulating "natural" pre-exploitation conditions, the entire flow system is initialized with a temperature of 240°C (464 F) and a corresponding saturated vapor pressure of 33.44 bars (485 psi). Initial water saturation is 80% in the background reservoir and 0% in the fracture. Boundary conditions in the background reservoir are held constant to initial conditions at the cylinder mantle (R = 1000 m = 3281 ft). Top and bottom boundaries are modeled as semi-infinite (thermally) conductive half-spaces. Lateral boundaries in the fracture are "no flow"; perpendicular to the fracture plane different boundary conditions were explored, including semi-infinite conductive half-spaces, and permeable matrix rock. The latter requires a fully three-dimensional fracture-matrix grid, while conductive boundary conditions can be efficiently modeled with a semi-analytical technique (Vinsome and Westerveld, 1980; Pruess and Bodvarsson, 1984; Pruess, 1991b).

The production well representing Q-6 is placed on deliverability, with mass flow rate given by

$$q = \sum_{\beta=liq.,\ gas} \frac{k_{r\beta}}{\mu_\beta} \rho_\beta \, PI(P_\beta - P_{wb}) \qquad (1).$$

Here k_r, μ, ρ are, respectively, relative permeability, viscosity, and density of fluid phases in the (fracture) production grid block. PI is the productivity index, a characteristic feature of the well reflecting permeability-thickness and skin (Coats, 1977), and P_{wb} is the flowing wellbore pressure. These parameters are here taken to be PI = 10^{-11} m^3 (35.3×10^{-11} cuft), and P_{wb} = 10 bars (145 psi). Prior to startup of injection we model an extended production period of 5 years, to simulate appropriate reservoir depletion in the area of the NCPA injection experiments. Subsequently water injection is started into the fracture at a distance of 240 m (787 ft) from the production well, and at the same elevation. Water at a temperature of 20°C (68 F) is injected at rates from 12-25 kg/s (191-397 gpm) for periods of from 1 to 3 days. During injection the production well continues to operate at the same deliverability conditions as before, with interference effects manifest in changing flow rates and enthalpies. The simulation is continued past the termination of injection to investigate recovery behavior. So far all of our simulations have only been performed for one single injection cycle; interference effects and constraints from repetition of many cycles have not yet been explored.

All calculations reported in this paper were done on an IBM RS/6000 workstation with LBL's general-purpose reservoir simulator TOUGH2 (Pruess, 1991b). This code incorporates the general "MULKOM" architecture for multiphase fluid and heat flow (Pruess, 1983b), and includes special provisions for modeling geothermal flows in fractured-porous media.

RESULTS AND DISCUSSION

Simulation results for an injection rate of 25 kg/s (397 gpm) and a 600 x 600 m^2 (3.88×10^6 sq. ft) fracture size are given in Figs. 5 through 12. Fig. 5 shows production rate vs. time for the periods before, during, and after injection. Fig. 6 shows the pressure distribution in the fracture at the end of a 5 year production period, prior to start of injection, for a case where the fracture has permeable wall rock. The fracture connection to the background reservoir in the bottom right corner is evident from the shape of the isobars. At the end of the 5 year production period, temperatures in the fracture are 240°C (464 F) throughout. In the background reservoir temperatures have declined somewhat from boiling, with lowest temperatures being approximately 234°C (453 F). Figs. 7-12 give contour maps of water saturations, temperatures, and pressures in the fracture. Results for different cases are summarized in Table 2. Simulated behavior can be briefly described as follows.

After production is first started at a time of -5 years, flow rate initially declines rapidly, and later stabilizes at rates of typically 9.5 kg/s (75,397 lbs/hr). Startup of injection causes rapid interference with production, due to a complex interplay between two-phase flow and heat transfer effects around the injection point (Calore et al., 1986; Pruess, 1991a). Heat exchange between the injection plume and the surrounding reservoir occurs partially through conduction, and partially through transport of sensible and latent heat and associated phase change processes. A boiling injection plume is a very efficient heat transfer system akin to a "heat pipe" (Calore et al., 1986). Reservoir vapor flows towards cooler, lower-pressure regions of the plume where it condenses, depositing large amounts of latent heat. In hotter regions of the plume the saturated vapor pressure exceeds ambient reservoir pressures, causing vapor to flow away from the plume, and inducing boiling. The concurrent condensation and boiling processes tend to diminish temperature variations throughout the injection plume.

Injected water migrates primarily downward and, near the bottom of the fracture, also laterally. Advancement of lower temperatures and pressures from the injection point is much delayed relative to water migration, due to the various heat transfer processes. In a recent study (Pruess, 1991a) it was shown that the simulated movement of injection plumes can be strongly affected by the orientation of the numerical grid, due to the gravitational instability of dense injection water over less dense steam. Test calculations showed that for the flow system modeled here grid orientation effects are insignificant. The reason for this favorable situation is the presence of a strong transversal dispersion in the descending plume, caused by conductive heat transfer from the fracture walls. Due to this heat transfer, the interior region of the plume beneath the injection point tends to have somewhat larger temperatures and pressures. This gives rise to a horizontal (outward) component of liquid (and vapor) flow, and a broadening of the injection plume.

Following start-up of injection the simulations show a brief initial period of increasing production rate. This occurs because initially the injected water is boiling at temperatures high enough so that the saturated vapor pressures exceed vapor pressures in the fracture prior to injection. Production rates then decline as large portions of the injection plume cool to temperatures with saturated vapor pressures lower than initial vapor pressures, inducing condensation of reservoir vapor.

For the simulations shown in Figs. 5-12, the vapor inflow from the background reservoir extends over a length of 120 m (394 ft) at the right lower boundary of the fracture. This path is just beginning to get blocked by injection water after 1.2 days (Fig. 7). At this time production rate has dropped to approximately 60% of the stabilized pre-injection value. The decline is caused by the partial blockage of vapor upflow, and by declining pressures from the cooling effects of injection. At 1.2 days, most of the outer envelope of the injection plume is at pressures of 22 bars (319 psi) or larger, corresponding to temperatures of > 217°C (423 F). After 3 days of injection, a plume of significant water saturations with $S_w > 0.5$ extends all the way across the lower third of the fracture, where it impedes vapor upflow. Pressures of the injection plume surface facing the production well region have declined to values of 16-20 bars (232-290 psi), with saturation temperatures of 201-212°C (394-414 F). Together these effects reduce production rate to less than 30% of the pre-injection value.

As is clear from the water saturation distributions (Figs. 7 and 10), no water breakthrough to the production well was observed in our simulations. However, water breakthrough would have occurred if the production well had been placed at lower elevation, or if injection had been continued for longer time periods.

Shutting-in of the injection well has an immediate impact on production, causing recovery and then over-recovery by about 10% over the stabilized pre-injection rate. It is seen that the permeability of the fracture wall rock, even when it is as low as 2 microdarcies, has a very significant effect. Impermeable wall rock can boil water only by heat conduction to the fracture. When wall rock is permeable it will imbibe injection water by capillary force. Boiling will then proceed at temperatures close to original reservoir temperature, and production rates exceeding stabilized pre-injection values are maintained for much longer periods of time. As long as injection continues the vapor generated in the reservoir rock adjacent to the fracture condenses in the cooler portions of the injection plume, slowing the temperature and pressure

decline there. When injection and further cooling stops, this vapor no longer condenses and becomes available for production.

The extent of flow rate decline during the 3-day injection period is excessive in comparison with the field observations. This may be attributed to a combination of several factors. The "real" fractures may be more extensive than the fracture in our model. In the field experiment, the injected water probably exited well Q-2 through several different fractures, whose combined heat transfer area is likely to be significantly larger than the surface area of the fracture in our model. Furthermore, not all of the fractures accepting injection water will also intersect Q-6, and not all of the fractures feeding Q-6 will intersect Q-2. Therefore, a reduction in production rate from one of the feeds of Q-6 will have a lesser relative impact on production than predicted from our single-fracture model.

Even in the case with dramatic production decline after 3 days of continuous injection, good recovery and over-recovery is observed when injection is stopped. This result is encouraging, indicating that even in cases with very strong negative injection interference production can be recovered by shutting-in the offending injector.

A limited number of variations in problem parameters and flow geometry have been explored. Table 2 summarizes simulated production interference and recovery for different fracture sizes. Injection rates and times, and permeability of the fracture walls, were also varied. In all cases stabilized production rate before start of injection was near 9.5 kg/s (75,400 lbs/hr). Production and injection were always made at the same elevation. As expected, smaller fractures produce more rapid and stronger negative interference with production, and less over-recovery. The permeability of the rocks forming the fracture walls is an important parameter. For impermeable wall rock the over-recovery following injection shut-in is very short-lived.

Different couplings between the fracture and the background reservoir were tried. Placing the coupling either beneath the injector or beneath the producer had very little impact on predicted production rates, although it did have some effects on the shape of the injection plumes. Similarly, introduction of non-zero capillary pressure in the fracture had negligible impact on production rates. There is considerable uncertainty about fracture relative permeabilities, and future studies should explore their sensitivity to production rates. Vapor pressure lowering effects have been neglected so far; as capillary effects are believed to be weak in fractures, vapor pressure lowering is also not expected to be significant.

CONCLUSIONS

(1) Our numerical simulation studies have predicted strong interference between injection into and production from the same fracture. During injection production rates mostly decline, with over-recovery observed after injection is stopped. The simulated behavior is similar to field observations in the Q-2/Q-6 experiments, lending credence to the underlying conceptual and numerical model.

(2) The most significant reservoir processes during injection include gravity-driven downward migration of injected water, local heat exchange with reservoir rock swept by the injection plume, conductive heat transfer from rocks of very low permeability to the injection plume, capillary-driven imbibition of injected liquid into the matrix rock, away from the fractures, vapor condensation in the cooler portions of the plume, and boiling in the hotter portions.

(3) The simulated production declines are stronger than seen in the field. This can be explained by noting that in our model all injected water enters one single fracture, and all production comes from that same fracture, whereas in the field several fractures will participate in taking up injectate, and delivering fluid and heat to the production well.

(4) The simulations clearly demonstrate that injection is subject to heat transfer limitations. Production rate decline from injection is caused primarily by temperature decline in the injection plume and associated drop in vapor pressure. Cool portions of injection plumes act as low-pressure sinks that can consume large amounts of vapor by condensation. Temperature decline depends on injection rate and on the heat transfer capacity of the reservoir, which is a function of available heat exchange volume, heat transfer area, and permeability for vapor flow.

(5) Based on the foregoing, it is to be expected that each injection well has a limitation on the rate at which water can be injected without causing significant reservoir pressure decline, and consequently negative interference with neighboring producers. Acceptable limits for injection rates may be difficult to predict, as they depend on geometric properties of the local fracture system that usually are poorly known. However, in practice such limitations can be established empirically by monitoring neighboring production wells.

(6) Injection should not be concentrated into a few wells that would take up large rates. Because of heat transfer limitations, injection wells should generally be operated at moderate rates well below their capacity for accepting fluids (Enedy et al., 1991).

ACKNOWLEDGMENT

The work presented in this paper was undertaken on the suggestion and with encouragement from Marshall Reed of the Geothermal Division, U.S. Department of Energy. The authors appreciate helpful discussions with Tom Box of Calpine Corporation. Peter Fuller and Curt Oldenburg of LBL provided a data interface for plotting simulation results. For a review of the manuscript, and the suggestion of improvements, the authors are indebted to Marcelo Lippmann. This work was supported by the Assistant Secretary for Conservation and Renewable Energy, Geothermal Division, of the U.S. Department of Energy under Contract No. DE-AC03-76SF00098.

REFERENCES

Beall, J.J. and Box, W.T. (1989), "The Nature of Steam Bearing Fractures in the South Geysers Reservoir," Geothermal Resources Council, Transactions, Vol. 13, 1989, pp. 441-448.

Beall, J.J., Enedy, S. and Box, W.T., Jr. (1989), "Recovery of Injected Condensate as Steam in the South Geysers Field," Geothermal Resources Council, Transactions, Vol. 13, 1989, pp. 351-358.

Calore, C., Pruess, K. and Celati, R. (1986), "Modeling Studies of Cold Water Injection into Fluid-depleted, Vapor-dominated Geothermal Reservoirs," paper presented at 11th Workshop on Geothermal Reservoir Engineering, Stanford University, Stanford, CA, January 1986.

Coats, K.H. (1977), "Geothermal Reservoir Modelling," paper SPE-6892, presented at the 52nd Annual Fall Technical Conference and Exhibition of the SPE, Denver, CO, October 1977.

Enedy, K.L. (1992), "The Role of Decline Curve Analysis at The Geysers," in: C. Stone (ed.), Monograph on The Geysers Geothermal Field, Special Report No. 17, Geothermal Resources Council, Davis, CA, 1992.

Enedy, S., Enedy, K. and Maney, J. (1991), "Reservoir Response to Injection in the Southeast Geysers," Proceedings, Sixteenth Workshop on Geothermal Reservoir Engineering, Stanford University, Stanford, CA, January 1991.

Goyal, K.P. and Box, W.T. (1990), "Reservoir Response to Production: Castle Rock Springs Area, East Geysers, California, U.S.A.," Proceedings, Fifthteenth Workshop on Geothermal Reservoir Engineering, Stanford University, Stanford, CA, January 1990.

Persoff, P., Pruess, K. and Myer, L. (1991), "Two-phase Flow Visualization and Relative Permeability Measurement in Transparent Replicas of Rough-walled Rock Fractures," LBL-30161, presented at Sixteenth Workshop on Geothermal Reservoir Engineering, Stanford University, Stanford, CA, January 1991.

Peters, R.R., Klavetter, E.A., Hall, I.J., Blair, S.C., Heller, P.R. and Gee, G.W. (1984), "Fracture and Matrix Hydrologic Characteristics of Tuffaceous Materials from Yucca Mountain, Nye County, Nevada," Sandia National Laboratory, Report SAND84-1471, Albuquerque, NM, December 1984.

Pruess, K. (1983a), "Heat Transfer in Fractured Geothermal Reservoirs with Boiling," Water Resources Research, Vol. 19, No. 1, February 1983, pp. 201-208.

Pruess, K. (1983b), "Development of the General Purpose Simulator MULKOM," Annual Report 1982, Earth Sciences Division, Lawrence Berkeley Laboratory LBL-15500, 1983.

Pruess, K. (1991a), "Grid Orientation and Capillary Pressure Effects in the Simulation of Water Injection into Depleted Vapor Zones," Geothermics, Vol. 20, No. 5/6, 1991, pp. 257-277.

Pruess, K. (1991b), "TOUGH2—A General-purpose Numerical Simulator for Multiphase Fluid and Heat Flow," Lawrence Berkeley Laboratory Report LBL-29400, May 1991.

Pruess, K. and Bodvarsson, G.S. (1984), "Thermal Effects of Reinjection in Geothermal Reservoirs with Major Vertical Fractures," Journal of Petroleum Technology, Vol. 36, No. 10, September 1984, pp. 1567-1578.

Pruess, K. and Narasimhan, T.N. (1982), "On Fluid Reserves and the Production of Superheated Steam from Fractured, Vapor-dominated Geothermal Reservoirs," J. Geophys. Res., Vol. 87, No. B11, 1982, pp. 9329-9339.

Pruess, K. and O'Sullivan, M. (1992), "Effects of Capillarity and Vapor Adsorption in the Depletion of Vapor-dominated Geothermal Reservoirs," Lawrence Berkeley Laboratory Report LBL-31692, presented at Seventeenth Workshop on Geothermal Reservoir Engineering, Stanford University, Stanford, CA, January 1992.

Pruess, K. and Tsang, Y.W. (1990), "On Two-phase Relative Permeability and Capillary Pressure of Rough-walled Rock Fractures," Water Resources Research, Vol. 26, No. 9, September 1990, pp. 1915-1926.

Thompson, R.C. and Gunderson, R.P. (1992), "The Orientation of Steam-bearing Fractures at The Geysers Geothermal Field," in: C. Stone (ed.), Monograph on The Geysers Geothermal Field, Special Report No. 17, Geothermal Resources Council, Davis, CA, 1992.

van Genuchten, M.Th. (1980), "A Closed-form Equation for Predicting the Hydraulic Conductivity of Unsaturated Soils," Soil Science Society Journal, Vol. 44, 1980, pp. 892-898.

Vinsome, P.K.W. and Westerveld, J. (1980), "A Simple Method for Predicting Cap and Base Rock Heat Losses in Thermal Reservoir Simulators," J. Canadian Petroleum Technology, July-September 1980, pp. 87-90.

Table 1: Specifications of numerical model (#)

FRACTURE ZONE

Vertical X-Z section, 0.1 m thick, 10 % porosity
Areal extent: variable, from 300 x 300 m^2 to 600 x 600 m^2
(984 x 984 to 1969 x 1969 sq. ft)
Permeability-thickness product in fracture plane: 40 darcy-meters
(131,200 md-ft)

Relative permeability: Corey-curves with $S_{lr} = 0.3$, $S_{gr} = 0.05$
Capillary pressure: 0

Wall rock: impermeable, or permeability = 2 microdarcy
relative permeability and capillary pressure: function of van Genuchten (1980), with parameters as measured for welded tuff sample G4-6 by Peters et al. (1984);
parameters: $\lambda = 0.4438$ $S_{lr} = .08$
$P_0 = 17.27$ bar (250 psi)
gas phase relative permeability: $k_{rg} = 1 - k_{rl}$

Discretization: 15x15x1 square blocks (for impermeable wall rock) 15x15x6 blocks (for permeable wall rock; increments perpendicular to fracture: .01 m, .19 m, .8 m, 4 m, 15m, for total wall rock thickness of 20 m)

BACKGROUND RESERVOIR

Radially symmetric layered system (2-D, R-Z), discretized into 5 layers and 16 radial blocks per layer.

Radius: 1000 m (3281 ft)

Layers (from top down)	Thickness		Permeability-Thickness	
1	20 m	(66 ft)	10 dm	(32,808 md-ft)
2	40 m	(131 ft)	4 dm	(13,123 md-ft)
3	80 m	(262 ft)	4 dm	(13,123 md-ft)
4	160 m	(525 ft)	1.6 dm	(5,249 md-ft)
5	200 m	(656 ft)	2 dm	(6,562 md-ft)
total	500 m	(1640 ft)	21.6 dm	(70,866 md-ft)

Porosity: 4 %

Relative permeability: function of van Genuchten (1980) for liquid;
parameters: $\lambda = .4438$
$S_{lr} = .80$ (*)
gas phase relative permeability: $k_{rg} = 1 - k_{rl}$

Capillary pressure: function of van Genuchten (1980);
parameters: $\lambda = .4438$ $S_{lr} = .08$
$P_0 = 1.727$ bar (25.0 psi)

Rock grain properties

density: 2600 kg/m^3 (162.3 lbs/cu-ft)
specific heat: 1000 J/kg°C (.239 Btu/lb x deg-F)
conductivity: 2.51 W/m°C (34.8 Btu/day x ft x deg-F)

(#) Initial and boundary conditions, and well parameters, are given in the text.

(*) Large irreducible water saturation, to approximate effective behavior of a dual-permeability medium (Pruess, 1983a).

Table 2. Injection-production interference. Simulated results for different fracture sizes, and injection rates and times.(*)

Fracture Size	Wall Rock (a)	Injection Rate	Production Interference (b)	Production Recovery (c)
300 m x 300 m	I	12 kg/s	64% at 0.5 days	99% at 1.7 days
450 m x 450 m	I	12 kg/s	80% at 1.2 days 42% at 10 days	110% at 2.0 days 105% at 15.9 days
600 m x 600 m	I	12 kg/s	91% at 1.2 days	113% at 2.0 days
	I	25 kg/s	66% at 1.2 days	113% at 2.0 days 102% at 3.5 days
	P	25 kg/s	60% at 1.2 days	111% at 2.0 days 109% at 3.5 days 103% at 10 days
			28% at 3.0 days	109% at 5.7 days 107% at 10 days

(*) All times relative to start of injection.
(a) I = impermeable wall rock, P = permeable wall rock with $k_m = 2$ μd.
(b) Interference is expressed as a percentage of pre-injection production rate.
(c) Recovery is expressed as a percentage of pre-injection production rate.

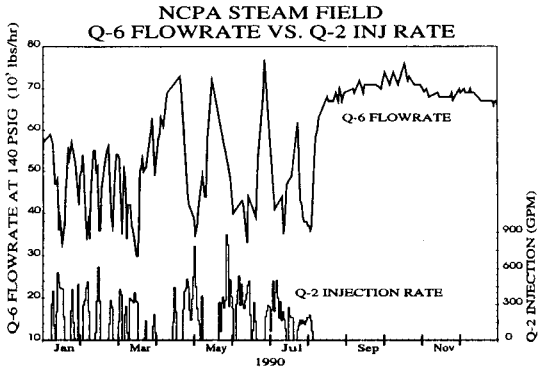

Figure 1. Injection rates into Q-2 and observed production from Q-6.

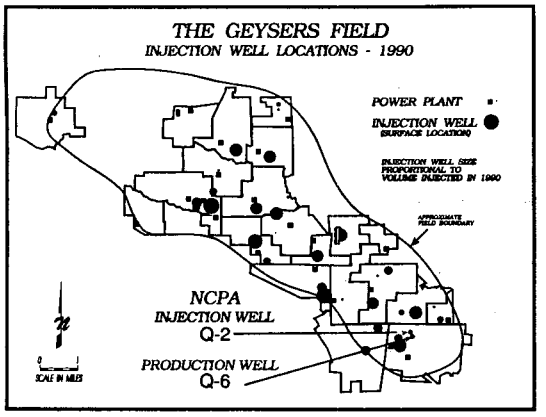

Figure 2. Injection well locations at The Geysers.

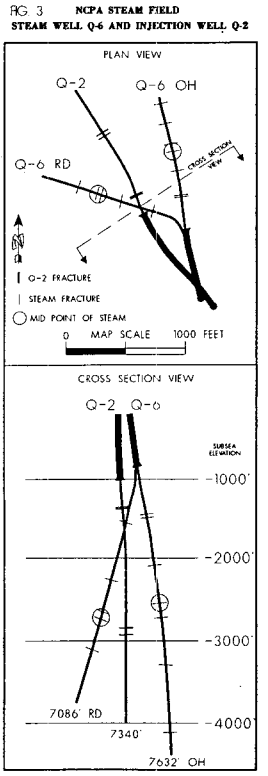

Figure 3. Plan and cross-sectional view of Q-2 and Q-6 well courses.

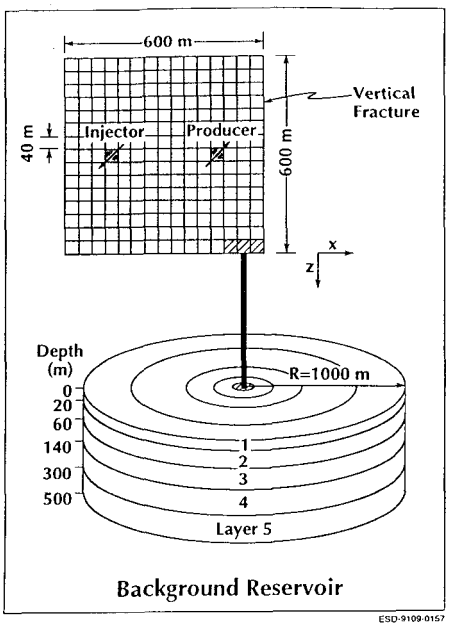

Figure 4. Schematic diagram of fractured reservoir model used in numerical simulations. Injection and production wells are intersected by the same vertical fracture, which is connected to a large background reservoir. Fluid and heat flow perpendicular to the fracture plane is also taken into account.

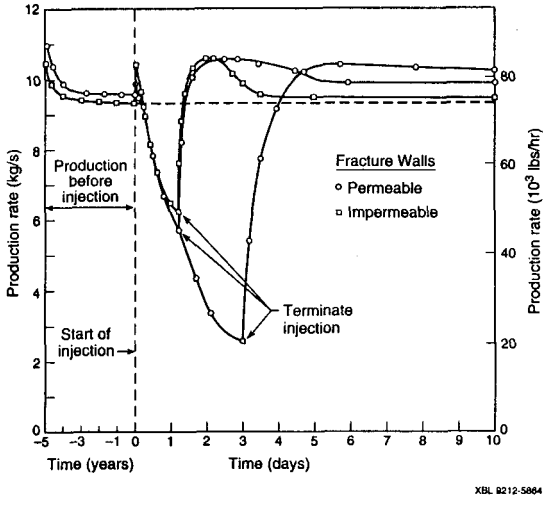

Figure 5. Production rate before, during, and after injection. Note the change of time scale at time = 0.

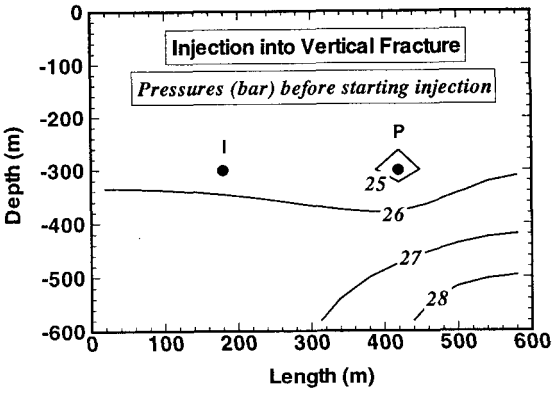

Figure 6. Vapor pressures in the fracture before start of injection, for a case with permeable fracture wall. I and P indicate the points where injector and producer penetrate the fracture.

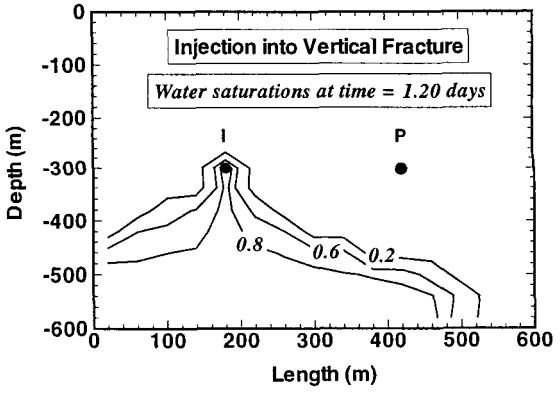

Figure 7. Water saturations in the fracture after 1.2 days of injection (impermeable fracture wall; I-injector, P-producer).

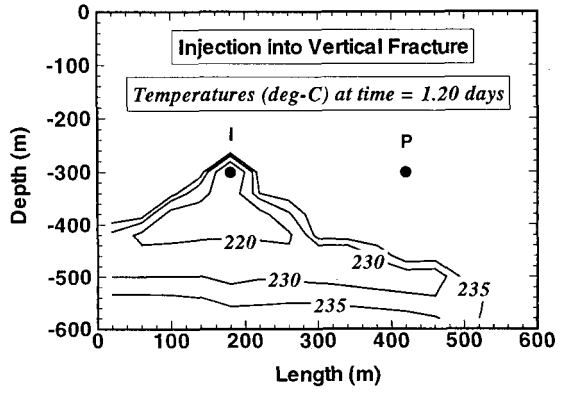

Figure 8. Temperatures in the fracture after 1.2 days of injection (impermeable fracture wall; I-injector, P-producer).

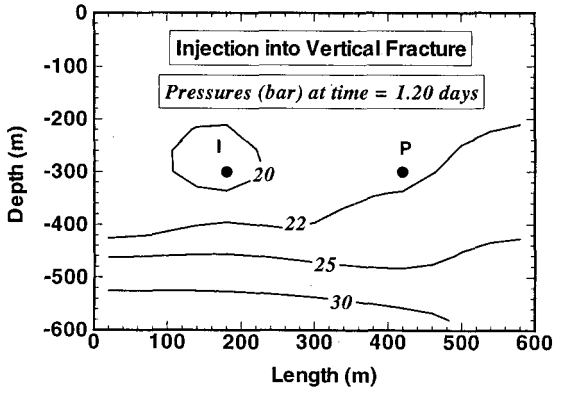

Figure 9. Fluid pressures in the fracture after 1.2 days of injection (impermeable fracture wall; I-injector, P-producer).

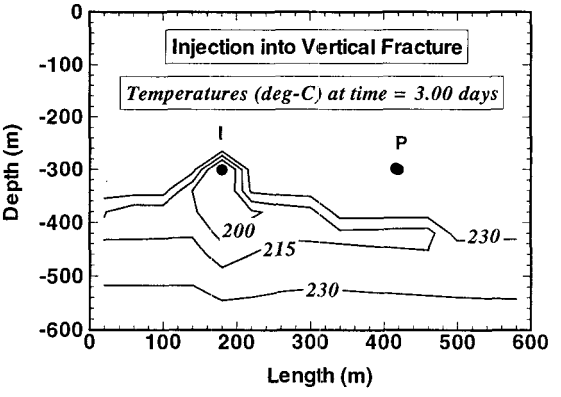

Figure 11. Temperatures in the fracture after 3.0 days of injection (permeable fracture wall; I-injector, P-producer).

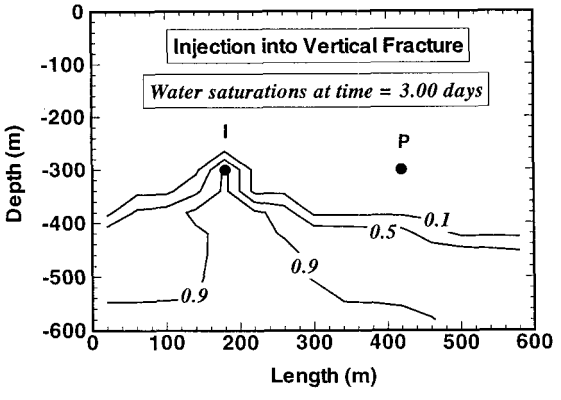

Figure 10. Water saturations in the fracture after 3.0 days of injection, case with permeable fracture wall; I-injector, P-producer.

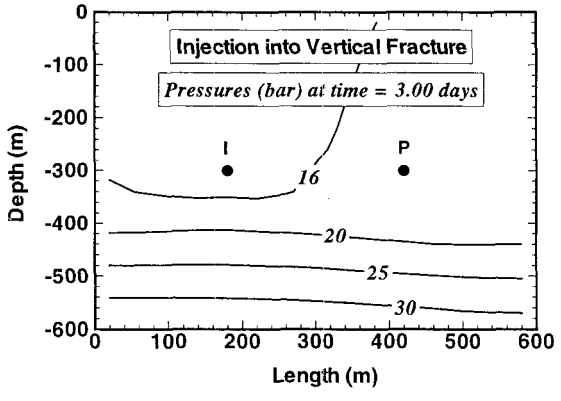

Figure 12. Fluid pressures in the fracture after 3.0 days of injection (permeable fracture wall; I-injector, P-producer).